VIKING ENTRY AERODYNAMICS AND HEATING
Robert J. Polutchko
Martin-Marietta Corporation

MR. POLUTCHKO: Entry into the relatively thin Mars atmosphere is pretty straightforward compared to some of the more exotic outer planet entries you have been hearing about. Figure 5-20 describes the characteristics of the Mars entry including the mission sequence of events and associated spacecraft weights.

The Viking spacecraft is comprised of a modified Mariner Orbiter and the Viking Lander Capsule. The Mars Orbit insertion weight is 5189 pounds. After separation of the entry vehicle, the de-orbit maneuver is performed by a low thrust, long burn time (15 minutes) propulsive maneuver. This propulsion system is a mono-propellant hydrazine system that is also used for reaction control during entry. During the coast period (3 to 6 hours) after de-orbit, the entry vehicle is oriented to an angle of attack of -20 degrees in order to align several entry experiments with the free-stream velocity vector. I will describe the locations of the entry science sensors in a moment.

Atmospheric entry is arbitrarily defined as 800,000 feet and the entry vehicle weight is 2060 pounds. At 0.05 G's deceleration the entry vehicle reaction control is switched from pitch, yaw and roll attitude hold into a rate damping mode for pitch and yaw. The Viking entry vehicle flies a lifting trajectory so roll attitude hold is maintained to control the lift vector.

Parachute deployment is provided by the guidance and control system radar altimeter at 24,900 feet. Depending upon the atmosphere encountered the mortar fire Mach number will be between 0.6 and 2.1. The aeroshell/heat shield is aerodynamically separated 7.0 seconds after mortar fire. The terminal propulsion engines are ignited at 3565 feet above the surface and the parachute and base cover are separated 2.0 seconds after engine start. The terminal propulsion system is also mono-propellant hydrazine and the engines are differentially throttled for pitch and yaw
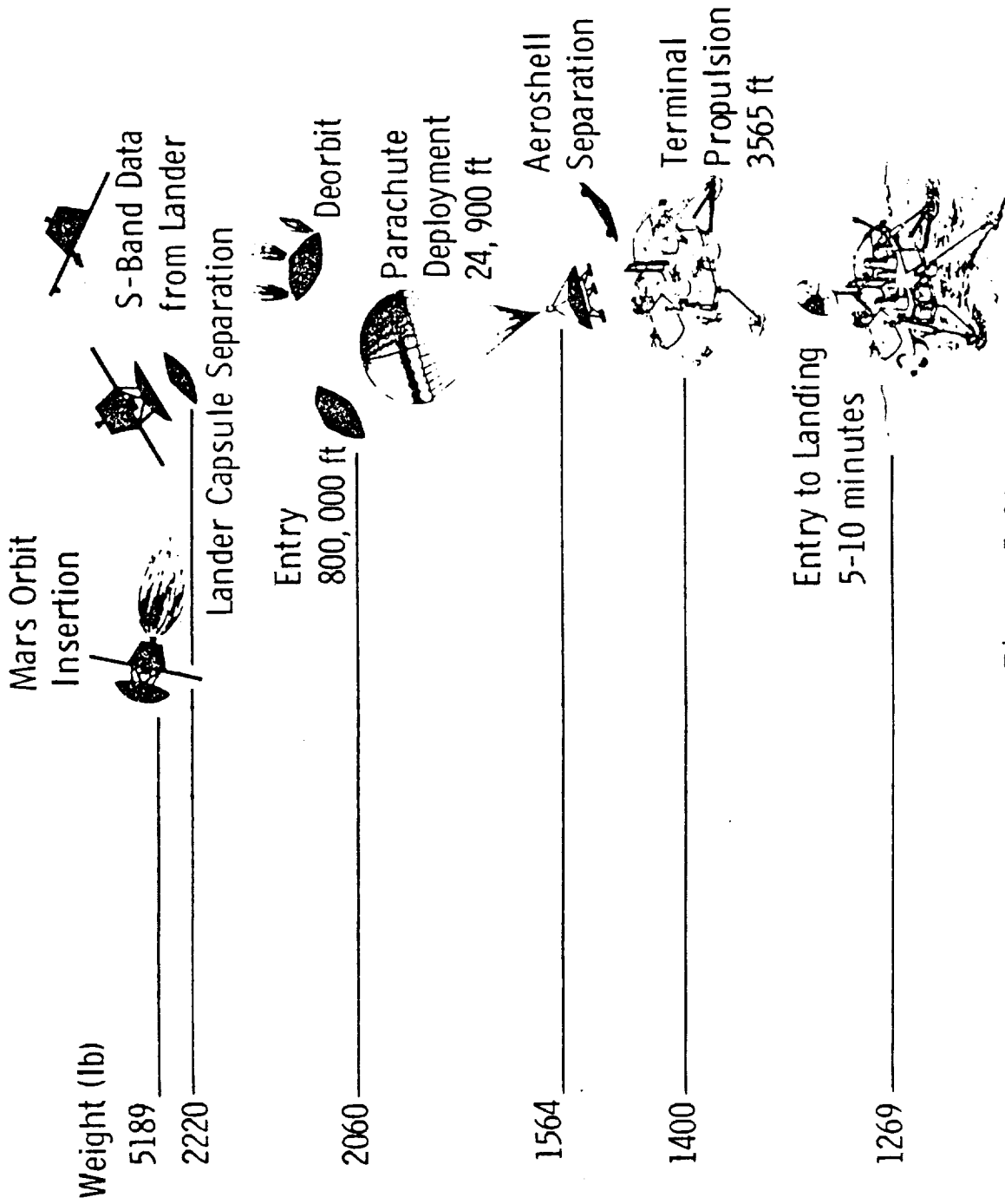
VIKING ENTRY THROUGH LANDING SEQUENCE

Mars Orbit Insertion

S-Band Data from Lander

Lander Capsule Separation

Entry 800,000 ft

Deorbit

Parachute Deployment 24,900 ft

Aeroshell Separation

Terminal Propulsion 3565 ft

Entry to Landing 5-10 minutes

Weight (lb)

5189

2220

2060

1564

1400

1269

Figure 5-20

control. Roll control is provided by small roll engines mounted on the terminal propellant tanks. A constant velocity descent contour is reached above the Mars surface and the Lander engines are cut-off at surface contact. The touchdown velocity will be approximately 8.0 feet/second.

The Viking entry into a relatively thin atmosphere is critically dependent upon high drag. The configuration as shown in Figure 5-21 is a 140-degree included angle cone with a base cover. There was, of course, considerable concern with the aerodynamic stability of very high drag configurations but we will discuss the stability characteristics in more detail later. The entry configuration is eleven and one-half feet in diameter. On the windward meridian several entry science instruments are located - an upper atmospheric mass spectrometer, a retarding potential analyzer and the stagnation pressure port. A stagnation (recovery) temperature sensor is located on the leeward meridian and is deployed through the heat shield at a velocity of 1.1 km/second (Mach 4.0). We also have some engineering measurements located on the heat shield (four diametrically opposed pressure ports) and one base cover pressure port.

Sometimes the more simple points are overlooked. For a very blunt vehicle lift is obtained from the high axial force. The body force diagram is shown in Figure 5-22. In order to obtain a positive lift from the axial force, a negative angle of attack is required. The normal force is also negative but is a small contributor to the resultant lift vector. For the Viking configuration the lift to drag ratio is given approximately by -0.015α. For a c.g. offset of -1.84 inches the trim angle of attack is -11.2 degrees and the L/D is 0.18.

Figure 5-23 presents test data for the aerodynamic characteristics of the entry vehicle showing trimmed alpha, drag coefficient and trimmed lift to drag ratio versus Mach number. The MD requirements here refer to the mission definition requirements for
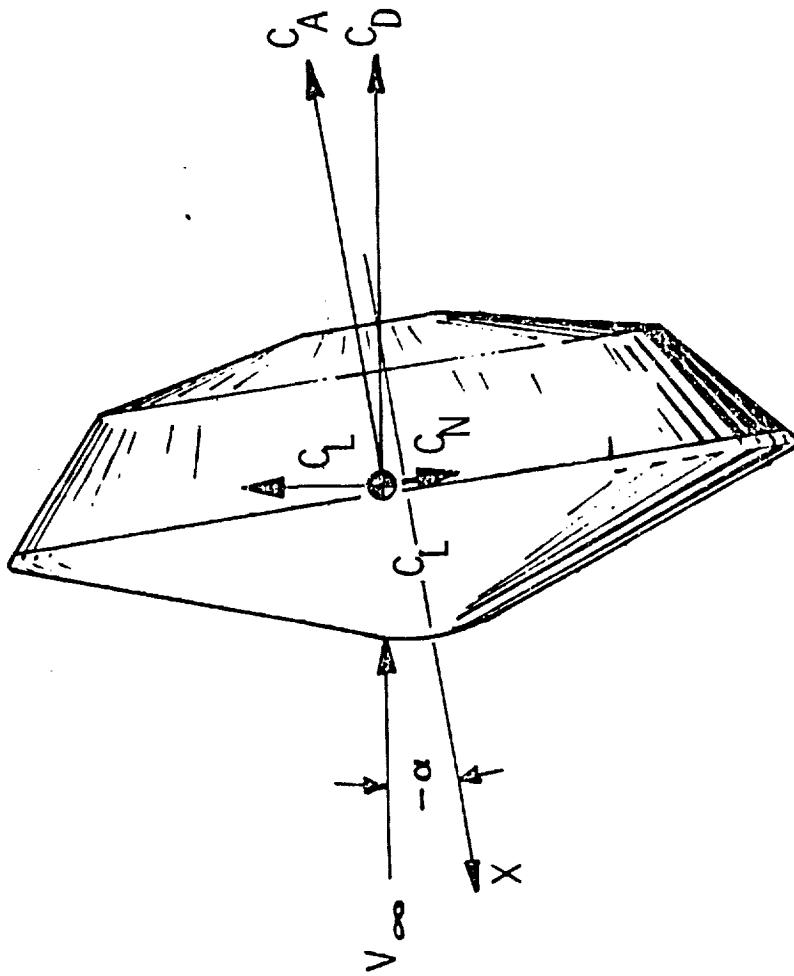
ENTRY VEHICLE CONFIGURATION DESCRIPTION
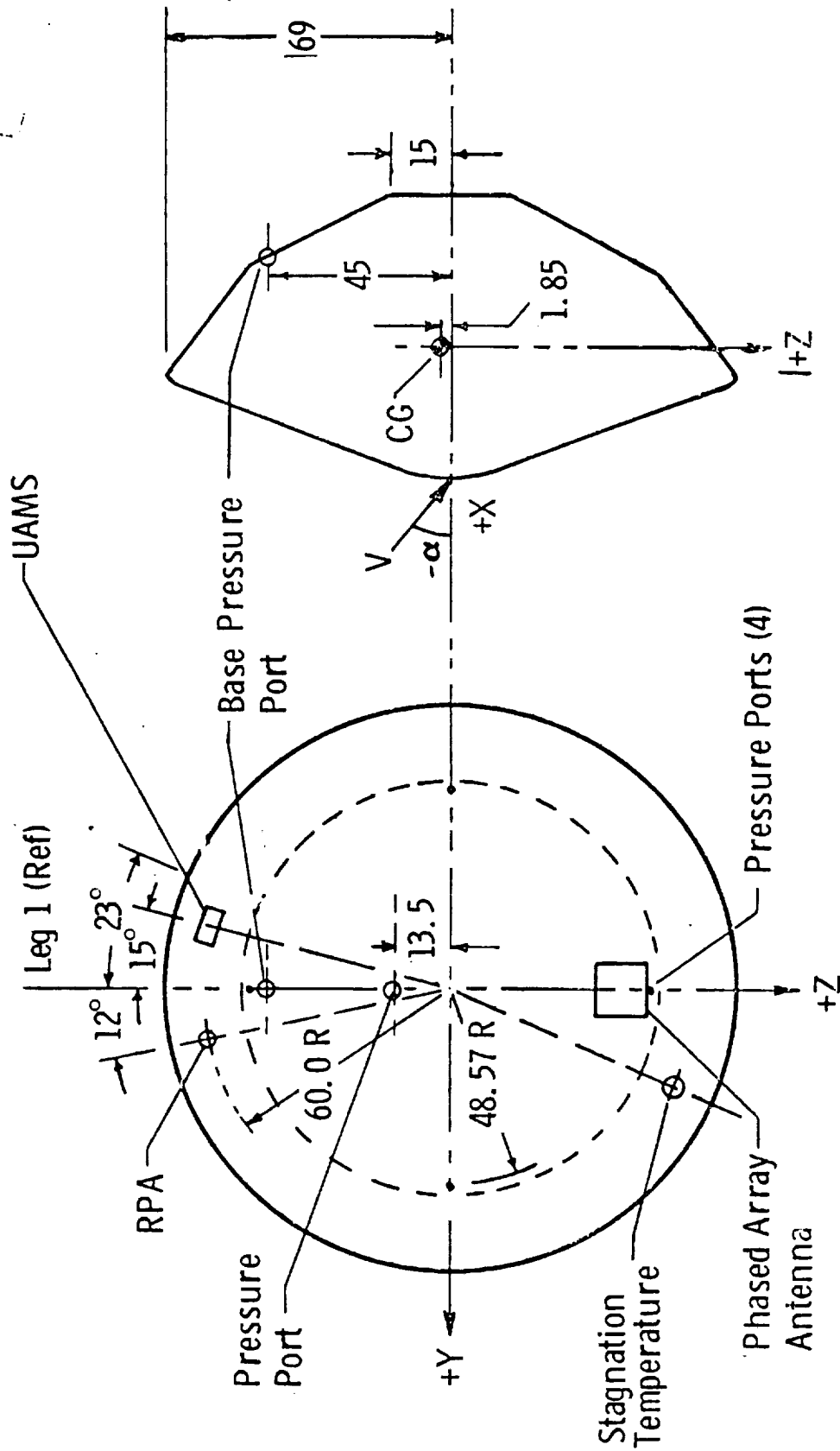
Note: All Dimensions in Inches

Figure 5-21

ENTRY VEHICLE BODY FORCES

$$C_L = C_N \cos \alpha - C_A \sin \alpha$$

$$C_D = C_N \sin \alpha + C_A \cos \alpha$$

$$\frac{L}{D} \approx \frac{C_{L_\alpha}(\alpha)}{C_D} \approx -0.015 \alpha$$

- Negative α Required for Positive Lift
- Negative α Obtained by CG Offset Above $\mathcal{C}$
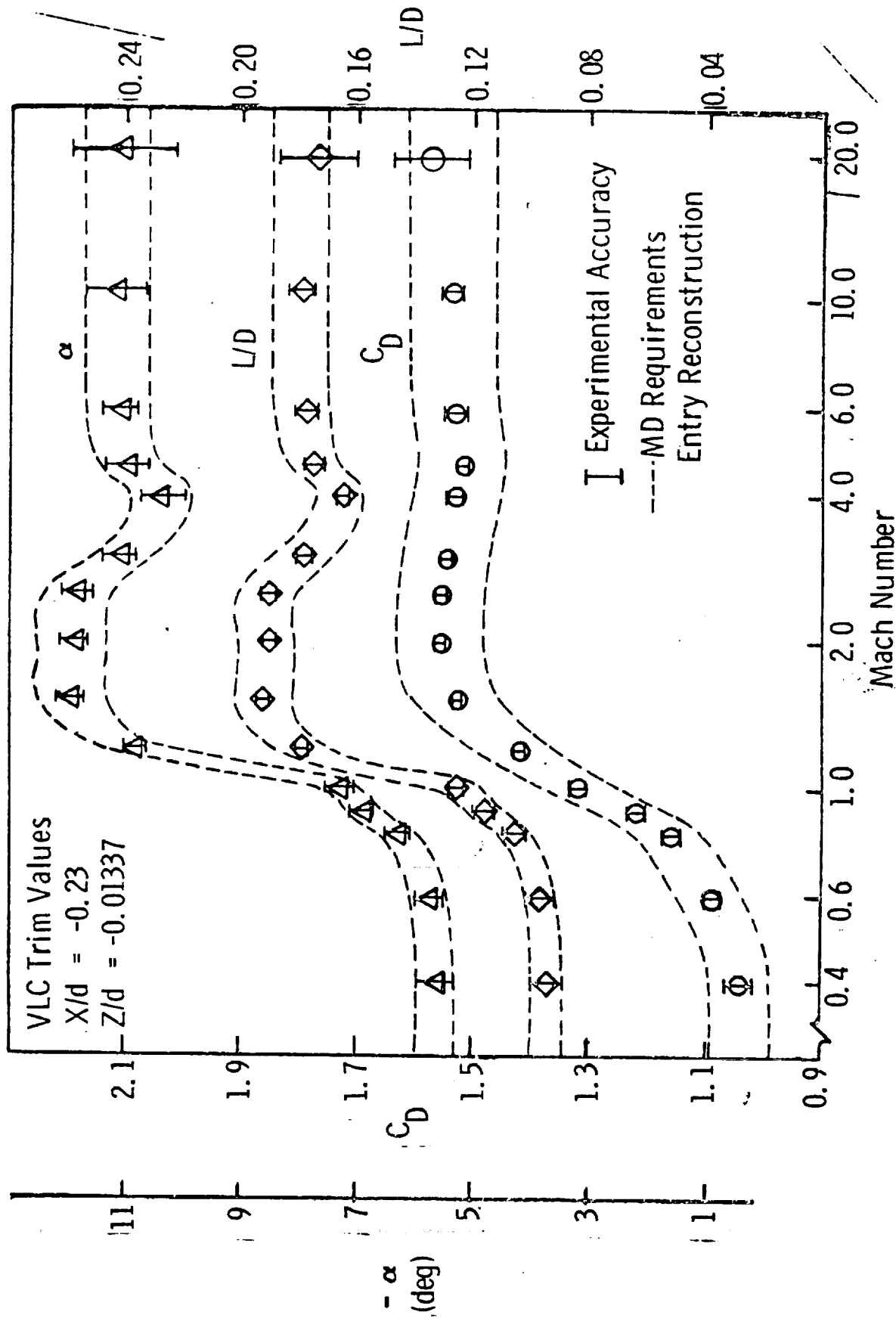
Figure 5-22

VLC WIND TUNNEL RESULTS

Figure 5-23

atmospheric reconstruction. The specification requires a priori aerodynamic coefficients within $\pm$ 5% and the test data certainly falls within the indicated tolerance. These test data were obtained using conventional wind tunnels and fairly straightforward testing technology.

Figure 5-24 shows the damping characteristics of the entry configuration. These data were experimentally derived utilizing forced oscillation and free oscillation testing techniques. This figure shows the basic negative damping at low angles of attack for very blunt configurations. The plots of C_{m_q} plus C_{m_α} versus α and the same parameter versus Mach number show that there are two Mach numbers (about 1.2 and 2.0) where we have negative damping at low angles of attack. It should be noted, however, that for a trim angle of attack of -11.0 degrees that the Viking configuration has positive aerodynamic damping at all Mach numbers. Also note the relative insensitivity of longitudinal c.g. position on the pitch damping values.

Al Seiff (NASA/ARC) is currently in the process of obtaining ballistics range (free flight) test data for the Viking configuration. Comparisons of foreced and free oscillation data with the free flight data should provide additional assurance of the predicted vehicle motions.

On Figure 5-25 the angle of attack time history is shown for several Viking entries. Again the entry altitude is defined as 800,000 feet above the mean surface level. As I mentioned earlier, the nominal trim angle of attack is -11.2 degrees when Viking enters the sensible atmosphere. At the end of the long coast period following the de-orbit maneuver the guidance and control uncertainty (worst case) in angle of attack is $\pm$ 10 degrees. For entry science reasons we have a pre-programmed attitude hold mode prior to entry into the atmosphere. The angle of attack will be -20 degrees which orients the windward meridian directly normal to the velocity vector for the mass spectrometer and RPA data. In the worst case then, alpha could be either -30 degrees or close
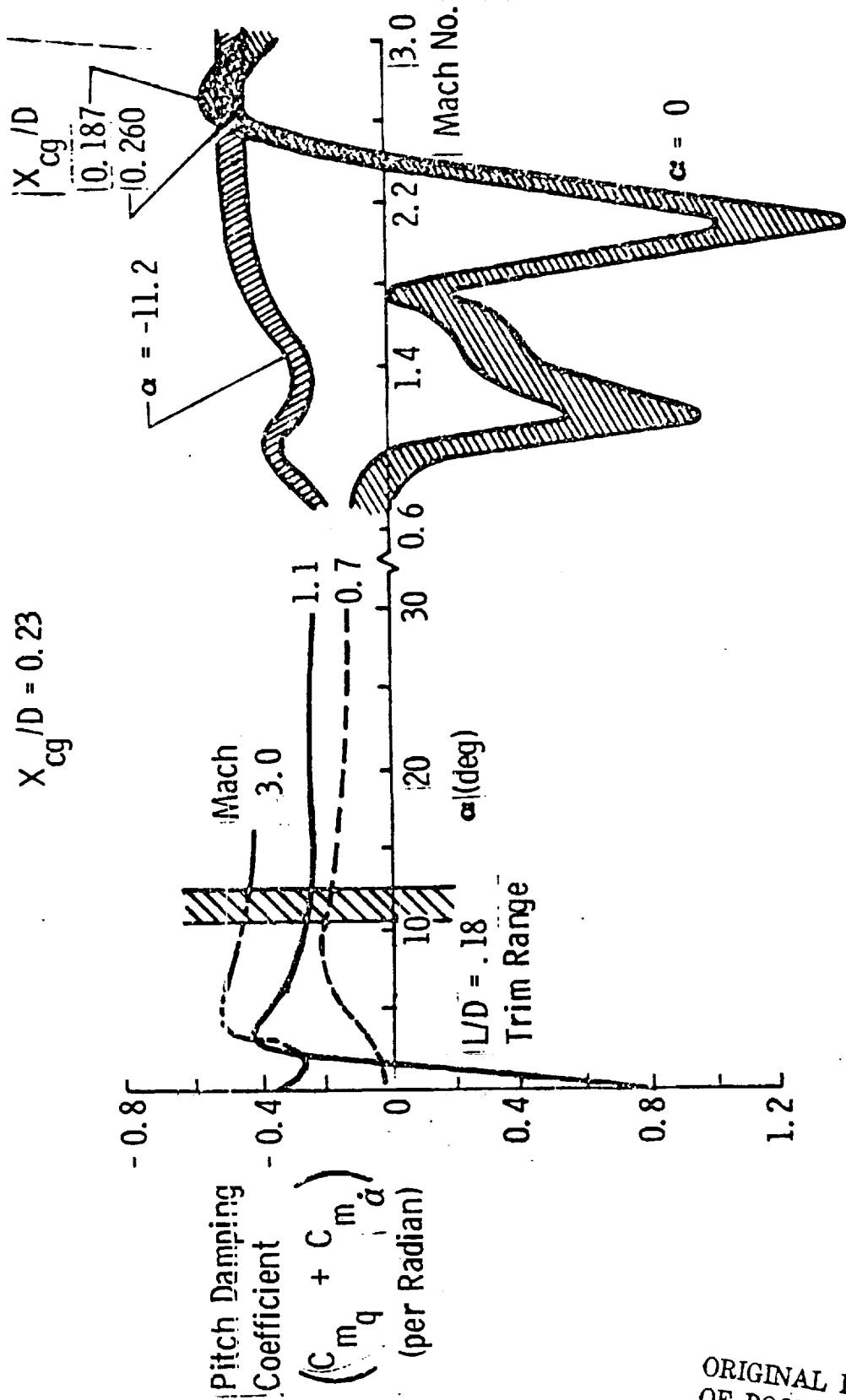
PITCH DAMPING CHARACTERISTICS
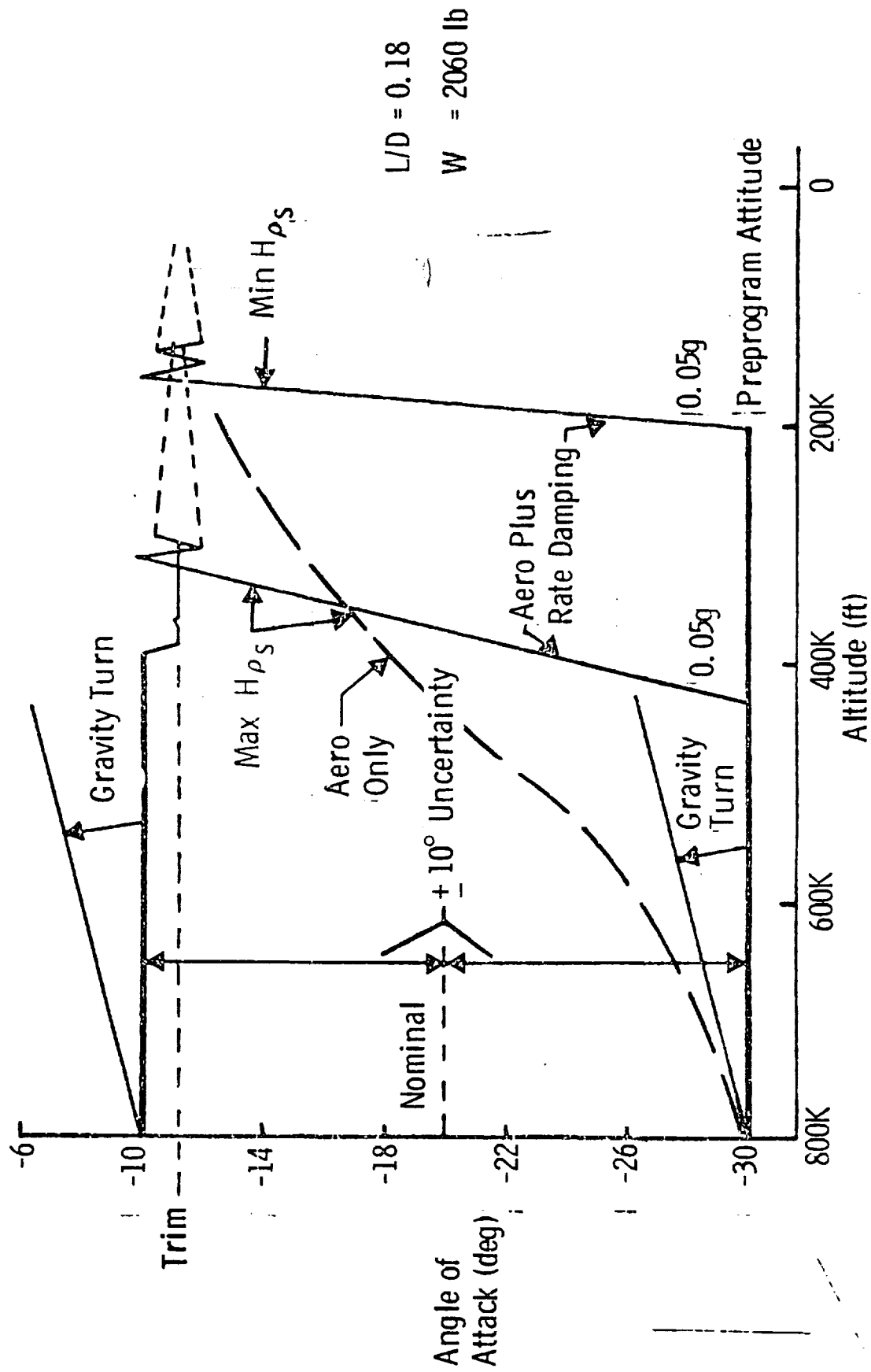
$$X_{cg}/D = 0.23$$

Figure 5-24

ENTRY DYNAMICS

Figure 5-25

to the trim angle. Our discussion here will be limited to the
-30 degree case.

A normal gravity turn will change the angle of attack as in-
dicated. At 0.05 G's we switch to rate damping and combined
with the natural aerodynamic damping characteristics the vehicle
motion rapidly converges to the trim alpha. Shown on this fig-
ure are two atmospheric extremes and the convergence associated
with only natural aerodynamic damping (i.e., reaction control sys-
tem inoperative). It should also be noted that the reaction con-
trol system is operating in opposition to the aerodynamic damping
forces in order to maintain the pre-programmed angle of attack.
These engines are 4 pounds of thrust each (4 engines). After
reaching the trim angle of attack maximum excursions due to spec
gust profiles (20 meters per second) show maximum excursions of
3 degrees to vehicle attitude.

Figure 5-26 presents the relatively mild stagnation heating
and pressure time histories. The curves are the worst case de-
sign limit values and represent atmospheric, entry angle and
lift to drag ratio extremes. The stagnation heating values are
calculated using a Newtonian pressure gradient and the Marvin
and Pope correlation with real gas effects included. This rela-
tively mild environment allows us to use very lightweight struc-
tures and heat protection and, therefore, the normal care of
design and test must be exercised to provide a minimum weight
entry vehicle.

Figure 5-27 presents the aeroshell heating distribution as
obtained in tests run in the NASA Ames 42-inch Shock Tunnel for
various gases. We also have obtained equivalent data in CF_4 at
NASA Langley and in air at Cornell. The solid curves are our
predictions of a heating distribution using the Aerotherm BLIMP
C program. All our data and predictions have correlated quite well
and an example of the agreement is given here. This high heating
rates at the corner of the aeroshell are caused in part by the
sharp radius - 1 inch full-scale. The differences indicated
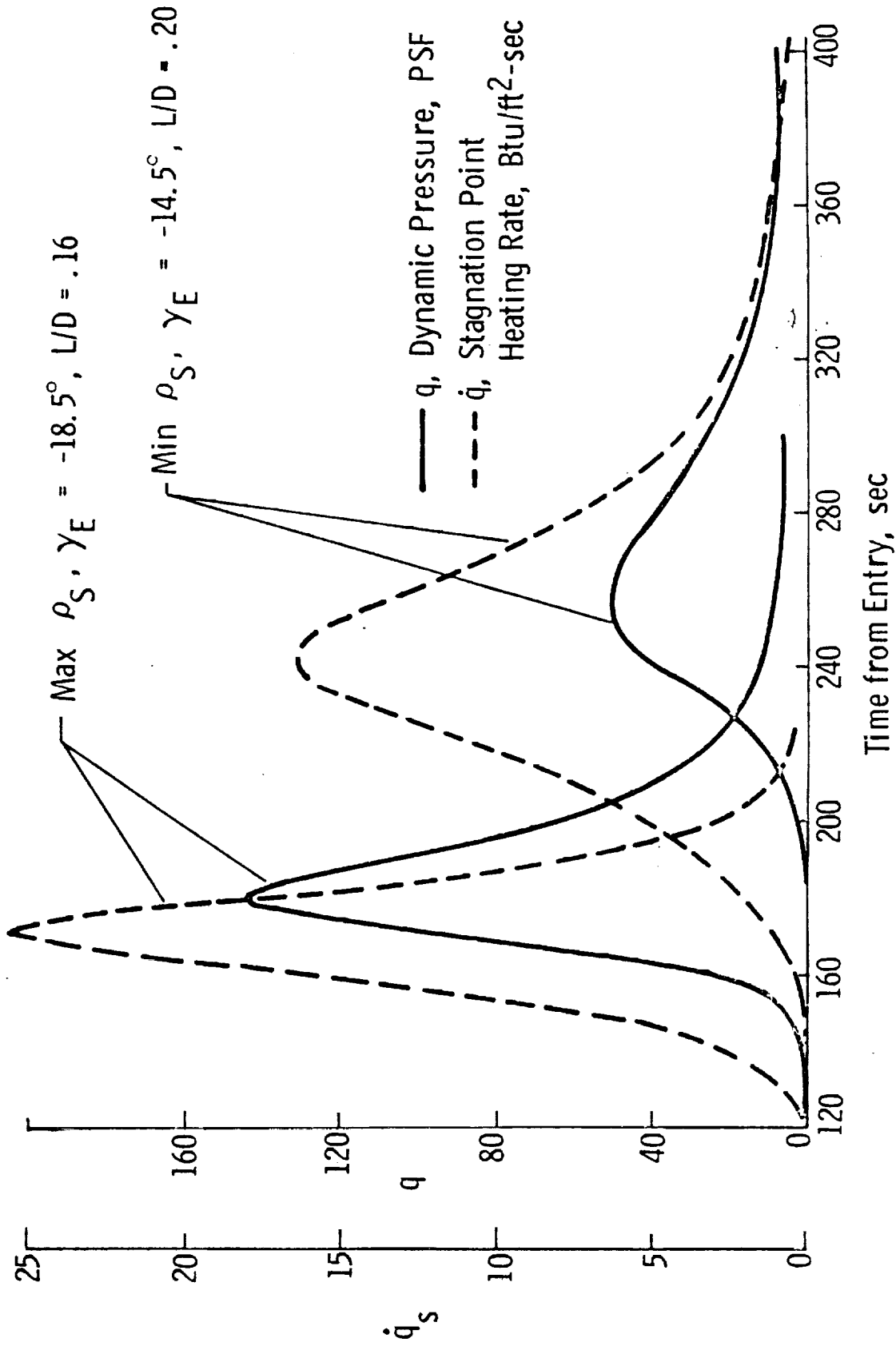
DYNAMIC PRESSURE AND STAGNATION HEATING HISTORIES

Figure 5-26

AEROHEATING DISTRIBUTION AND REAL GAS EFFECTS

Preliminary Data
Ames 42 in. Shock Tunnel

α	M	GAS
$\triangle$ -10°	15	Air
$\square$ -10°	15	100% CO_2
$\circ$ -10°	16	0.73 CO_2, .27 Ar
— -8.4°	20	Air, BLIMPC Program

Note: $\dot{q}$ = Local Heating Rate
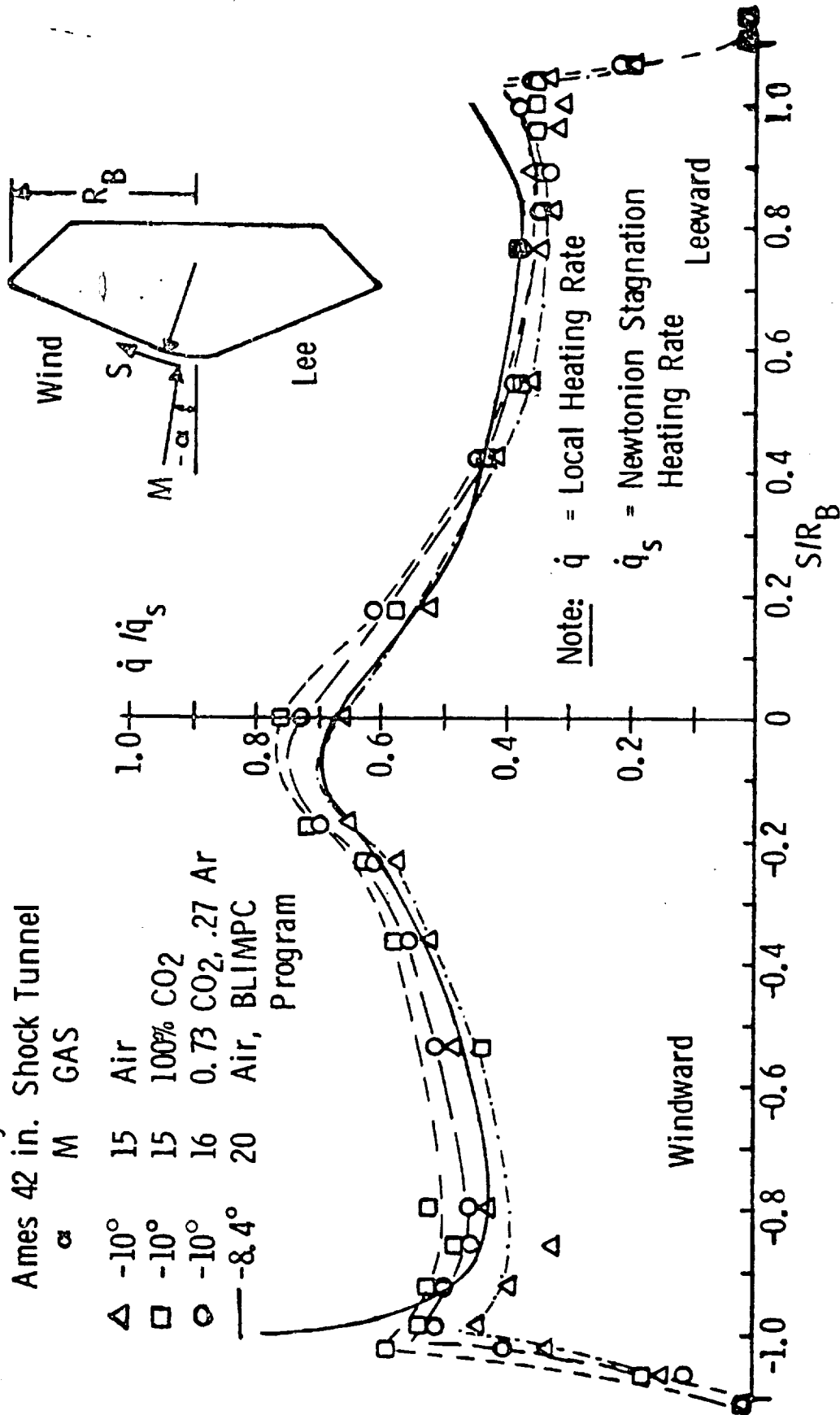
$\dot{q}_s$ = Newtonion Stagnation Heating Rate

Figure 5-27

between the BLIMP C prediction and the data is test model peculiar. We have obtained data on a model constructed to emphasize specifically the instrumenting of the sharp corner. These data indicate that the BLIMP predictions shown here are accurate. These predictions here are based on the pressure distribution data from that special model and the heating rates indicated by the test data shown here are, in fact, in error.

On Figure 5-28 is presented some heating data from the Variable Density Tunnel at Langley at Mach 8.0 in air. Also shown are BLIMP laminer and turbulent heating rate predictions. The leeward side of the aeroshell seems to experience a transition to turbulence at Reynolds numbers between 3 and 4 million. We artificially tripped the boundary layer and experienced additional increases in the local heating rates which seem to show a good resemblance to the turbulent predictions. The Viking Reynolds number at the peak heating point in the worst case trajectory is about 3 million and the evidence seems to indicate that we could expect transition on the leeward side. This Reynolds number translates to a momentum thickness Reynolds number of about 140.

Precise transit criteria is not the point here since many factors influence determination of such a specification. However, this wind tunnel test, in fact, was a very close flight simulation for Viking and in the same facility Apollo tests showed remarkable correlation with flight test data. The Viking heat shield was designed to handle the situation indicated by these data. We also placed the entry science recovery temperature sensor on the leeward meridian to take advantage of the higher local Reynolds numbers at that location.

The curve of Figure 5-29 presents the design values selected for the heat protection system based upon all the test data and analyses we have performed. Basically, we have taken a conservative approach that calculates the expected heating rates in the

VIKING TRANSITION STUDY

$\alpha = -11.2°$, Air
LRC VDT, M = 8.0

Sym	α	$Re_\infty \times 10^6$
○	+11.2	3.78
♂	-10.4	3.74
●	+ 9.5	3.74
□	+10.6	2.78
◇	-11.6	2.80

BLIMP Turbulent

Artificially Tripped

BLIMP Laminar

Windward

Leeward S/R$_B$

q/q$_S$

Figure 5-28

V-60
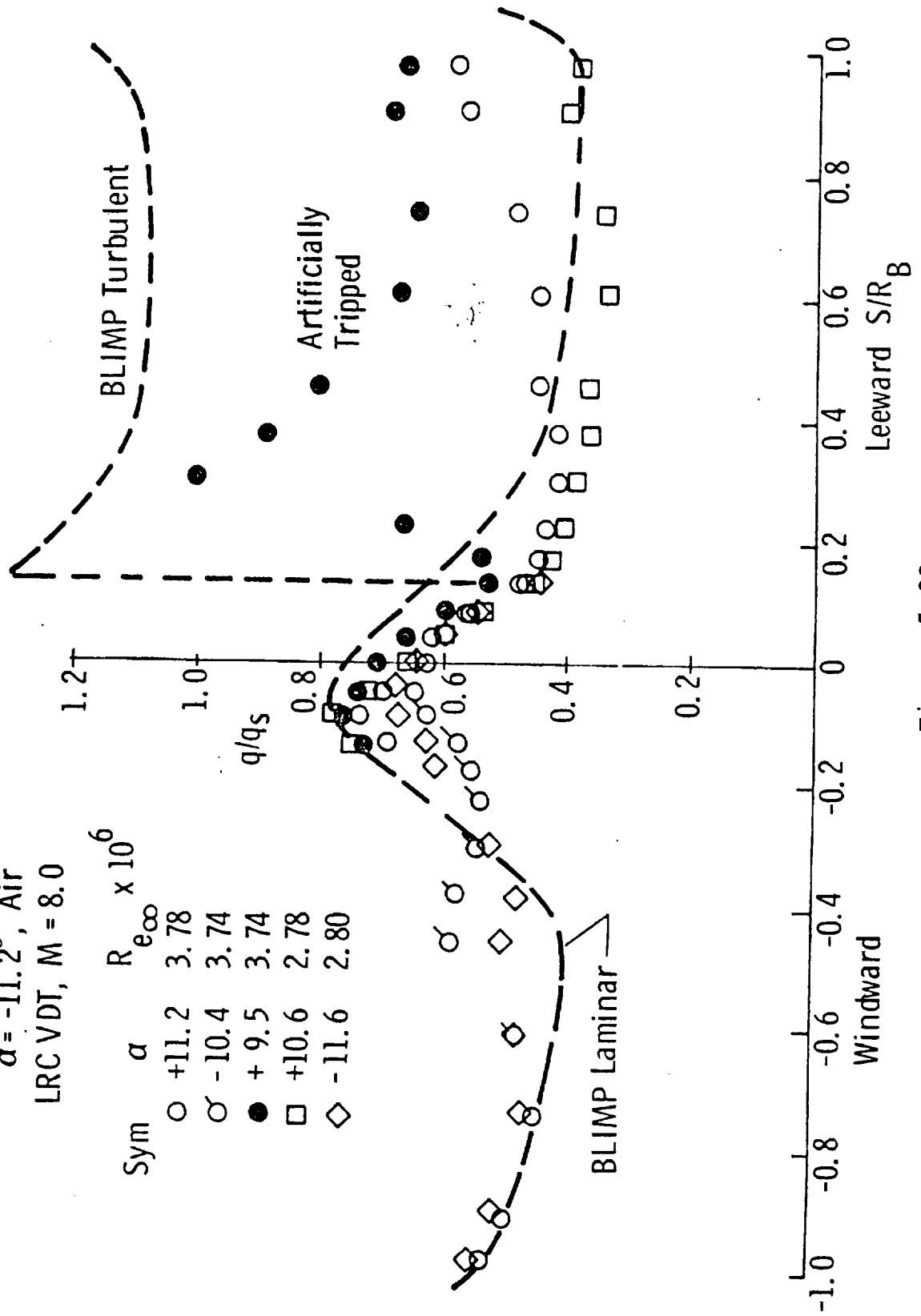
AEROSHELL DESIGN HEATING PITCH PLANE DISTRIBUTION

L/D = 0.16
α = -11.2°
γ_E = -18.5°
Max ρ_s Atmos
t = 172 sec (Peak Heating)

Note: Basecover Design Heating is 2% of Stagnation

Turbulent

Transitional

Laminar

$\dot{q}/\dot{q}_s$

1.4
1.2
1.0
0.8
0.6
0.4
0.2
0

Windward
1.0 0.8 0.6 0.4 0.2

Leeward
0 0.2 0.4 0.6 0.8 1.0
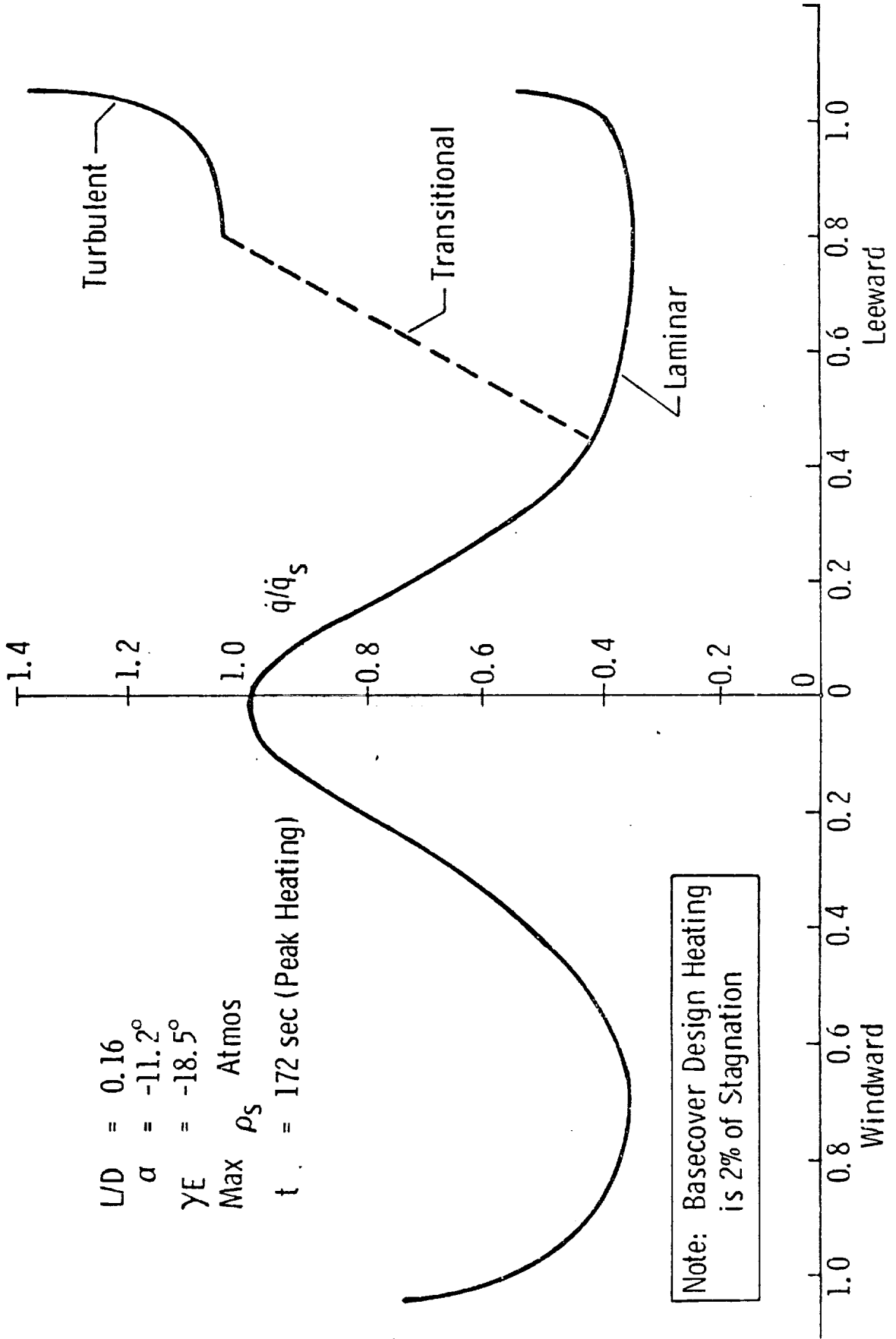
Figure 5-29

Mars CO_2 atmosphere by using a measured freon pressure distribution. The shock density ratio basically governs the pressures and the values for freon and CO_2 are very similar. For the turbulent areas we have modified the heating values using BLIMP rather than, for example, the Harris model at LRC. BLIMP gives a factor of three increase in this area while the Harris model shows about a factor of two. The stagnation area does not really experience a "Newtonian" stagnation heating rate but we have used the full stagnation value for design.

Figure 5-30 shows some test data we obtained on protuberances. The case shown here is the mass spectrometer cap which is potentially the largest if it failed to jettison prior to entry. The interference factor above the local "smooth" heating rate is plotted versus streamline direction. It can be seen that a factor of about 3.0 increase in heating rate could be expected. We have locally protected these areas with a high density ablative material that was previously flown on the USAF PRIME vehicle.

Figure 5-31 presents the real gas effects on the entry vehicle aerodynamics based on CF_4 data we measured at NASA-LRC and some preliminary data measured at NASA-ARC. You will note the slight increase in drag and the more non-linear nature of the pitching moment with alpha. However, the trim angle of attack for all three test gases is virtually the same for the Viking configuration at -11.2 degrees and the lift to drag ratio is virtually identical. We don't anticipate any problems for the lifting entry aerodynamic performance in the Mars atmosphere.

Figure 5-32 summarizes several of the design values and design factors for the Viking entry mission. The heat shield is basically an insulator and is, therefore, total heat rather than heating rate sensitive. The base cover is designed for 2 percent of stagnation heating based upon test data. The maximum base cover heating rate that was measured was 1.5 percent of stagnation. We have applied a design factor of 1.5 to all heating rates for smooth areas and a factor of 4.0 to all protuberances areas. Shear
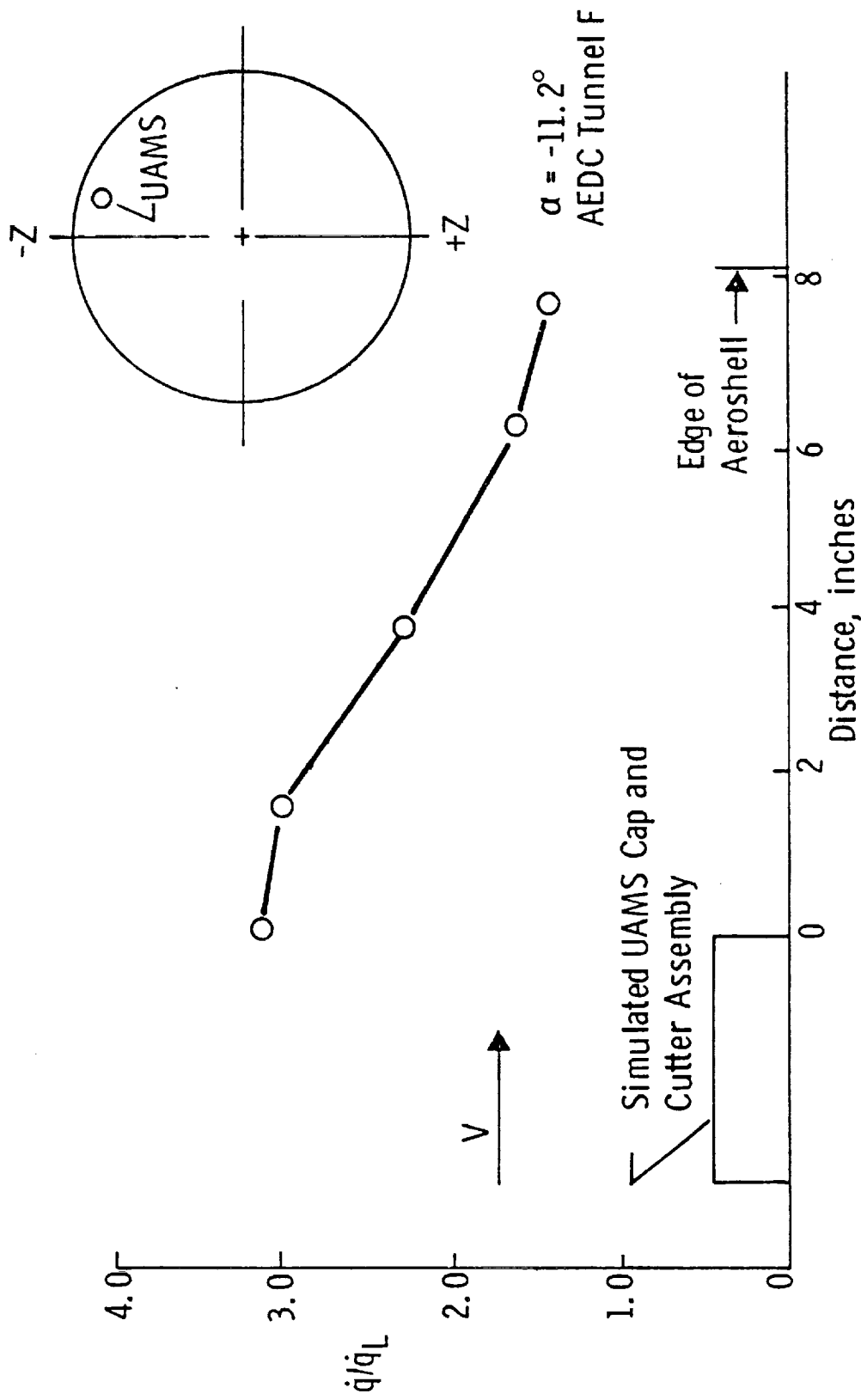
PROTUBERANCE HEATING EFFECT ON AEROSHELL

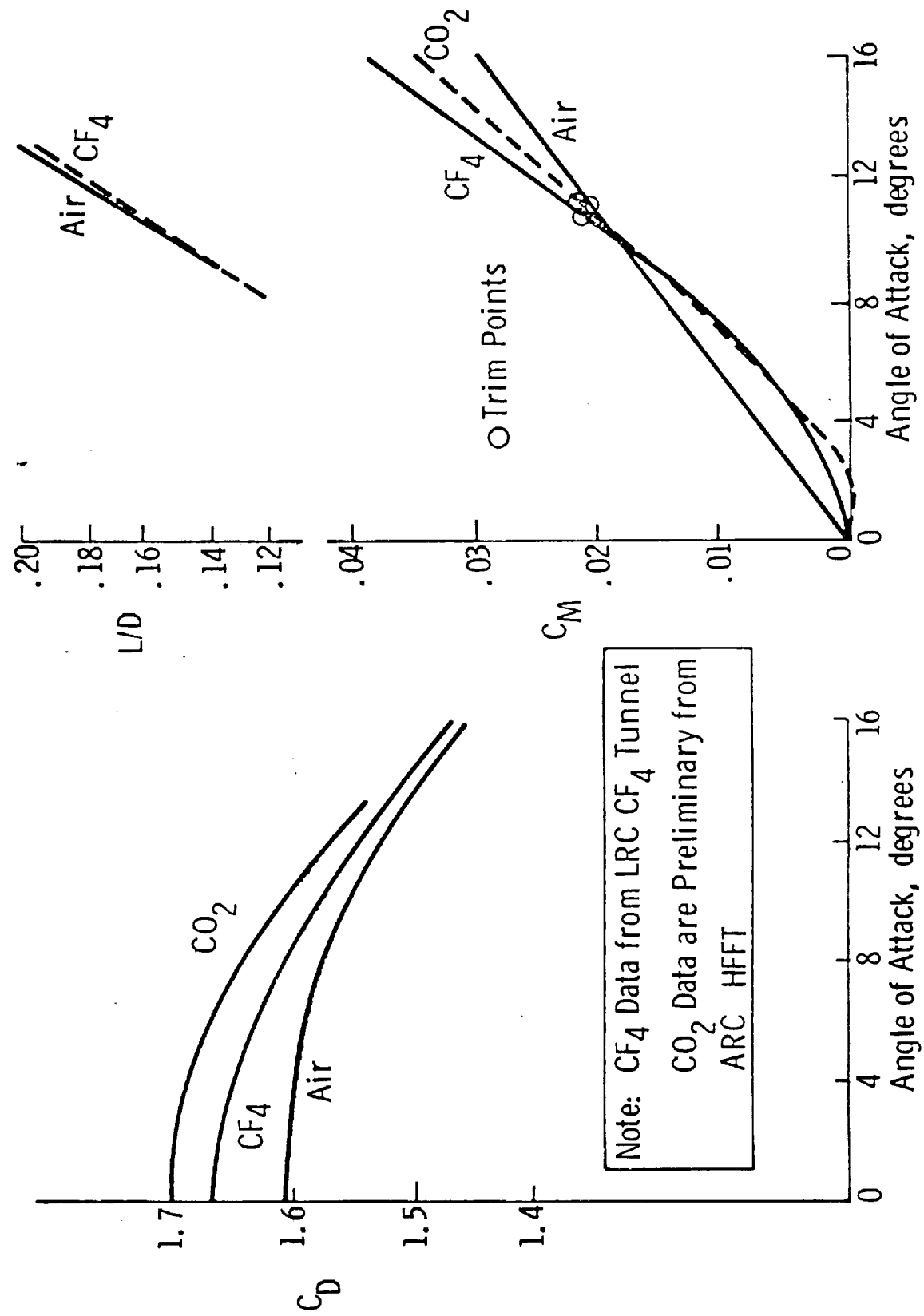Figure 5-30

EXPERIMENTAL REAL GAS EFFECTS ON AERODYNAMICS

Note: CF_4 Data from LRC CF_4 Tunnel
CO_2 Data are Preliminary from
ARC HFFT

Figure 5-31

V-64

ENTRY DESIGN VALUES AND DESIGN FACTORS

PARAMETER	AEROSHELL	BASECOVER	UNITS
Heating Rate (Smooth)	25.6	0.512	Btu/ft^2 - sec
Total Heat	1240	24.8	Btu/ft^2
Max Shear Stress	2.6	0	PSF
Dynamic Pressure	144	–	PSF
Load Factor	12.7	12.7	Earth G
Collapse Pressure	280.0	16.5	PSF

DESIGN FACTORS

Heating (Smooth Areas)	1.5
Heating (Protuberances)	4.0
Shear Stress	1.5
Collapse Pressure	1.25

CONSIDERATIONS

Atmosphere Extremes
$\gamma = -14.5°$ to $-18.5°$
L/D = 0.16 to 0.20
W = 2060 lbs
V_E = 15,175 FPS

Figure 5-32

stress factor is 1.5 and aerodynamic loads factor is 1.25. These
factors are applied to worst case combination of atmosphere model,
entry angles and lift to drag ratios.

I would now like to show you a five minute film clip of the
qualification flight test program of the Viking decelerator sys-
tem, the Balloon Launched Decelerator Tests, BLDT. As summarized
on Figure 5-33, the program consisted of four tests conducted at
the White Sands Missile Range (WSMR) in New Mexico and were de-
signed to span the extremes of the worst case conditions on Mars.
These flight tests also demonstrated the aerodynamic separation
of the full-scale aeroshell and the flying qualities of the entry
configuration in an uncontrolled mode.

The parachute is a disk-gap-band configuration 55 feet in dia-
meter, mortar deployed in a single stage with a mortar ejection
velocity of about 100 feet per second. Tests were conducted at
Mach numbers of 2.2, 1.2 and 0.5 and dynamic pressures of 14.5
and 4.5 pounds per square foot. The full-scale Viking test ve-
hicle was carried to 120,000 feet by a helium filled, 34 million
cubic foot balloon. The test vehicle was dropped from the bal-
loon and rocket boosted to the test altitude and Mach number. All
tests were successful and demonstrated a 35% structural margin
above the worst case expected at Mars.

BALLOON LAUNCHED DECELERATOR TESTS (BLDT)

Five Minute Test Sequence Film

Four Decelerator Qualification Flights over White Sands Missile Range (WSMR)

Mach Numbers from 0.5 to 2.2

Dynamic Pressures from 4.5 to 14.5 PSF

Test Altitudes from 90K to 150K feet

Balloon Altitude 120K feet

Aeroshell Separations at Mach $\approx$ 1.0

Figure 5-33